Observing the adsorption process of friction modifier additives by combination of quartz crystal microbalance (QCM-D) and confocal laser scanning microscopy (CLSM)

Jennifer Eickworth[1], Martin Dienwiebel[1,2], Thomas Rühle[3], Patrick Wilke[3]

1 Fraunhofer IWM MikroTribologie Centrum, Wöhlerstraße 11, 79108 Freiburg, Germany

2 Karlsruher Institut für Technologie KIT, Kaiserstraße 12, 76131 Karlsruhe, Germany

3 BASF SE, Carl-Bosch-Straße 38, 67036, Ludwigshafen, Germany

KEYWORDS

lubricants, friction modifier, QCM-D, CLSM, deposition

ABSTRACT

Friction modifier additive technologies play a crucial role in minimizing friction and wear of lubricated tribological systems. Present efforts to improve the energy efficiency and new

regulations require a fundamental understanding of the adsorption processes. Therefore, *in-situ* and oil compatible methods are needed.

This work combines the in-situ measurement of friction modifier additives deposition onto a surface and the resulting viscoelastic properties (using a quartz crystal microbalance with dissipation, QCM-D) with the imaging of the deposition process employing a fluorescence confocal laser scanning microscope CLSM). This approach enabled us to for the first time to observe the deposition *in-situ*.

Contrary to the common assumption present for almost 100 years that friction modifiers form monolayers, our CLSM-study shows that friction modifiers can also forms droplets in the mineral base oil and subsequently stay in the shape of a droplet after deposition on the Fe_2O_3 surface. The adsorbed droplets have diameters between < 1 µm and 127 µm. Small droplets are not mobile after deposition, but droplets with a certain diameter become mobile and move along the surface to merge with other mostly smaller droplets. We also find that droplets in solution prefer coalescence with already adsorbed droplets over deposition. From distribution and size of the adsorbed droplets, the adsorbed amount is calculated and correlated with the values found with QCM-D.

Hence, the combination with QCM-D the ongoing processes can be described quantitative and qualitative to give completely new insights in the deposition processes.

INTRODUCTION

The main classes of friction modifiers can be roughly divided into organic friction modifiers (OFM), functionalized polymers, soluble organo-molybdenum additives and dispersed nanoparticles [1]. Besides fatty acids, OFM's can comprise of carboxylates, alcohols, imides, borates, phosphorus compounds, ionic liquids, amides and amines [2].The adsorption mechanism and mode of action of fatty acids was in the focus of numerous studies during the last century (e.g. [3-8]) and the friction reduction is often explained using the boundary lubrication model that goes back to Hardy in 1922 [9]. The ongoing trend towards low-viscosity oils in order to reduce liquid friction losses increases the requirements especially for friction modifier additives, as friction must remain low even in the mixed lubrication regime. Moreover, as fatty acids can be corrosive and can cause damage, amines and their derivates are a promising alternative. Therefore more recently, research on OFM has gained new interest and the adsorption behavior of amines has been reported in literature as well, but not to such extent as fatty acids. This lack of knowledge and more stringent environmental guidelines motivated us to seek a better understanding of the adsorption of amine based friction modifiers.

Benítz et al. [10] studied the formation of self-assembled monolayers of octadecylamine on mica surfaces using chloroform as hydrophobic solvent with an atomic force microscope (AFM). The mica surfaces were immersed in 15 mM solutions (0.4 wt.%) at RT, removed and dried with N_2. Octadecylamine forms 0.3 µm to 0.5 µm wide and 1.6 nm high islands on the mica surface. Friction maps showed that the friction is reduced in the area of the islands. Ripening of the formed islands in air lead to larger islands, which indicates a certain mobility of the islands. Longer immersion times produce much more but smaller islands [10].

Zhu et al. [11] used a surface forces apparatus (SFA) modified for oscillatory shear tests to study the nano-rheological properties of hexadecylamine solved in tetradecane. The "hard-wall film thickness" was determined to be 4.7 nm (for 0.1 wt.% solutions) resulting from hexadecylamine molecules adsorbed at both mica surfaces (1.8 nm each) and 2 to 3 layers of randomly oriented molecules in between. In the oscillatory shear tests pure tetradecane showed a stick-slip transition and a limiting shear stress of 6.5 Pa, whereas the addition of 0.1 wt.% hexadecylamine did not show stick-slip and did reduce the limiting shear stress to 5.4 Pa.

The investigations of *Wood et al.* [12] and *Doig and Camp* [13] were more application-oriented as they used iron oxide surfaces. *Wood et al.* studied the hexadecylamine adsorption from hexadecane using polarized neutron reflectometry (PNR) and X-ray photoelectron spectroscopy (XPS) on an iron oxide layer (mixture of Fe_2O_3 and Fe_3O_4). For low amine concentrations, 1 and 4 x 10^{-4} mol/dm³ (0.02 and 0.1 wt.%) the layer thickness was found to be 1.6 nm. Higher concentrations, 1 and 4 x 10^{-3} mol/dm³ (0.24 and 0.97 wt.%) slightly increase the film thickness to 2 nm. As the length of an extended hexadecylamine molecule is 2.15 nm [14] the adsorbed molecules are supposed to be tilted by 42° (for 1.6 nm thickness) and 22° (for 2 nm thickness). For XPS analysis, an iron oxide surface was treated with 1.03 wt.% solution of hexadecylamine in hexadecane. The N1s emission line shows three peaks. The main peak results from the reaction of the amine with the surface and *Wood et al.* expect the nitrogen to donate an electron to the iron oxide surface and chemisorb, which means that the polar head groups are located at the iron-oil interface (classic thin film brush model for friction modifiers) [11]. *Doig and Camp* performed MD simulations under the same conditions as *Wood et.al*, to compare experimental and simulation data. The calculated values for the film thicknesses are in good agreement with the experimental data and were found to be 1.5 nm and 2 nm. From radial distribution functions it was shown, that the

positions of the head groups are prescribed by the lattice of the iron oxide surface, but that the ordering strongly decreases with a larger distance from the surface [13].

Except the work of *Zhu et.al.*, all presented investigations are ex-situ studies. *Eriksson* [15] and *Nalam et al.* [16] performed *in-situ* studies using the quartz crystal microbalance (QCM) with stainless steel coated quartz sensors. *Eriksson* studied the adsorption of tertiary amine ethoxylate and primary oleyl amine from commercially available group III engine oil. The QCM tests were performed at 50 °C and a flow rate of 250 µl/min. The amine ethoxylate adsorbs with 100 ng/cm² from a 1 wt.% solution and the oleyl amine with 27 ng/cm² from a 0.5 wt.% solution [15]. *Nalam et al.* found adsorbed amount in the same order of magnitude for a di-fatty amine (39 ng/cm²), a charged di-fatty amine (40 ng/cm²), a tri-fatty amine (46 ng/cm²) and a branched tri-fatty amine (58 ng/cm²) from 0.5 wt.% solutions in hexadecane. The corresponding layer thicknesses are in the range of 0.46 nm to 0.71 nm and the authors suggest the molecules to adsorb with a certain tilt angle or even parallel to the surface [16].

The presented research clearly shows the research gap when it comes to the combination of qualitative and quantitative studies. QCM is a powerful tool to investigate adsorbed amount, but does not provide information about the morphology of the adsorbent. All calculations to find film thicknesses are based on the model of monolayer adsorption, although the imaging of an adsorbed amine film with AFM showed island growth (cf. Ref. 10). Most of the research was performed using model fluids as solvents and friction modifiers.

This apparent predicament is in the center of our study, which is why we combined quantitative QCM measurements with qualitative fluorescence confocal laser scanning microscope (CLSM)

imaging, in order to investigate the deposition process of a commercially employed friction modifier from a group II mineral base oil.

EXPERIMENTAL

MATERIALS

We used a commercially available friction modifier (IRGALUBE® FE 1), which is an organic compound whose chemistry is broadly described in Ref. 17. We will abbreviate the additive as FA in the remainder of the paper. The relevant physical properties are given in Table 1. The head group can be a propyl group, an ester group or an alcohol group. The concentration of the FA was set to 1 wt.% for all measurements. As solvent a pure group II mineral base oil was used, abbreviated as BO. - As a non-polar reference oil a PAO 6 was used.

Table 1. Physical properties of FA, BO and BO + 1 wt.% FA

	FA	BO	BO + 1 wt.% FA
kinematic viscosity [mm²/s]	290 (20 °C)	25.48 (55 °C)	25.94 (55°C)
density [g/cm³]	0.97 (20 °C)	0.84 (55 °C)	0.84 (55°C)

As surfaces for the QCM-D experiments commercially available Fe_2O_3-coated 5 MHz quartz crystals with a roughness of 1.7 ± 0.1 nm (Biolin Scientific GmbH, Gothenburg, Sweden) were used.

METHODS

Quartz Crystal Microbalance with Dissipation (QCM-D)

The QCM measurements are performed using a QSense E4 (Biolin Scientific GmbH, Gothenburg, Sweden). The cell temperature is set to 55 °C and the oil is pumped through the cell using a peristaltic pump (Cole-Parmer GmbH, Wertheim, Germany). Each measurement starts with a non-polar reference oil to find the base line. After equilibrating the system, the following sequence is used for rinsing: 30 min reference oil, 30 min BO, 60 min BO + 1 wt.% FA, 30 min BO, 30 min reference oil. The flow rate is 130 µl/min[1]. For the present work only the rinsing steps 30 min BO, 60 min BO + 1 wt.% FA, 30 min BO are relevant, therefore the results are normalized to the BO as base line (Δf and ΔD are set to zero).

The signals used from the QCM-D are the frequency changes Δf and the dissipation shifts ΔD. Δf can be converted in a mass change Δm using the Sauerbrey equation [18]:

$$\Delta m = -c \cdot \Delta f \tag{1}$$

The proportionality constant or mass sensitivity constant c can be calculated from the thickness and intrinsic parameters of the crystal. For 5 MHz AT-cut quartz crystals, the Sauerbrey constant is $c = 17.7\ ng/(cm^2 \cdot Hz)$ (for details and parameters see e.g. Ref. 19). The calculation of adsorbed masses using the Sauerbrey equation can only be regarded valid if the following conditions are fulfilled: (1) the adsorbed masses are small compared to the weight of quartz crystal: $\frac{\Delta f}{f} \ll 1$ [19], (2) the adsorbed masses are distributed homogeneously on the surface, as the mass

[1] The used peristaltic pump Ismatec IPC (Cole-Parmer GmbH, Wertheim, Germany) is set to 200µl/min, calibrated for water.

sensitivity is Gaussian-shaped and has its maximum in the center [20], and (3) the adsorbed masses form rigid, non-deformable films on the surface and therewith have small dissipation shifts: $\Delta D \leq 10^{-6}$ [19,21]. For the tested systems, the 2nd and 3rd conditions are not fulfilled as we learn later that the adsorbed mass is not evenly distributed and ΔD is much higher ($\Delta D \approx 460 \cdot 10^{-6}$). To overcome these issues, Reviakine et. al. discussed different evaluation methods for QCM-D measurements and different types of layers [22]. For evaluating the adsorbed layer thickness, a distinction is made between homogeneously distributed layers and monolayers of discrete particles or other nanometer-sized adsorbents. In the case of homogeneous layers, in addition to the Sauerbrey approach for rigid films, the Kelvin-Voigt model for viscoelastic layers is commonly used. For discrete adsorbents in the form of droplets, bubbles or other objects, an FEM simulation of the hydrodynamics can be performed with detailed knowledge of the particle size and shape, as well as the surface coverage and mechanical properties [22, 23]. At this point, it becomes clear that the interpretation of QCM-D data without an additional imaging method is difficult, if not impossible, since it must first be known what type of film is formed and which approach is the correct one for this specific case. Since imaging is not always possible, a heuristic approach can be used in which the $\Delta D_n/-\Delta f_n$ - ratio is plotted over the negative frequency shift -Δf/n [23]. This approach is again subject to 3 conditions:

1. The negative $\Delta D_n/-\Delta f_n$ - ratio shows a linear negative slope with increasing negative frequency shift -Δf/n.

2. The slope becomes steeper for larger harmonics n.

3. The linear extrapolations converge on the X-axis on a common X-axis intercept.

4. The particles are small compared to the decay length of the oscillation (see below, formula 3).

The frequency shift $-\Delta f/n_{\Delta Dn=0}$ (X-axis intercept) can be converted into a radius r_{QCM} using the Sauerbrey constant c and the density of the adsorbent ρ_{ads} and formula 2.

$$r_{QCM} = \frac{\Delta f/n_{\Delta D=0} \cdot c}{\rho_{ads}} \tag{2}$$

Reviakine et. al. were able to determine the height of adsorbents using this approach for the absorption of liposomes on TiO_2 [24], while Tellechea et. al. additionally showed that the negative $\Delta D_n/-\Delta f_n$ ratio increases for larger particles but decreases again with increasing surface coverage [25]. The acoustic thickness of a layer, i.e., which can be measured by the QCM-D, depends on the size and on the distribution or surface coverage of the discrete adsorbents. Different combinations of size and distribution or surface coverage can thus lead to the same acoustic thickness [25].

The oscillation of the quartz sensors has a decay length δ into the immersed liquid that depends on the viscosity ϑ_l and the densityρ_l. Specifically, the oscillation (angular frequencyω) decays with [19] in the z-direction, i.e. perpendicular to the surface:

$$\partial = \left(\frac{2 \cdot \vartheta_l}{\omega \cdot \rho_l}\right)^{0.5} \tag{3}$$

Thus, films with a thickness lower than the decay length are detected fully (finite thickness), whereas films with a lager film thickness than the decay length (semi-infinite thickness) can be detected partially [19]. The decay lengths for the 5th overtone (f_5 = 25 MHz) for the measured liquids result from the given physical values and equation (2) to 0.57 µm for BO and to 0.58 µm BO + 1 wt.% FA.

Confocal Laser Scanning Microscopy (CLSM)

For the CLSM measurements a *Leica SP5 DM6000 B* (Leica Microsystems GmbH, Wetzlar, Germany) with a *HC FLUOTAR L 25x/0.95 W VISIR* objective (Leica Microsystems GmbH, Wetzlar, Germany) was used. The SP5 is an upright microscope system with a lateral resolution of maximum 200 nm. For the experiments, a flow cell with a geometry close to the QCM-D (true to scale replica) was used. The schematic of the measurement setup is depicted in Figure 1. The oil is pumped through the cell with a flow rate of approximately 130 µl/min. The cell is first filled with BO to ensure the sealing and wetting of the Fe_2O_3 surface. The Fe_2O_3 surfaces are the same as in the QCM-D measurements but the quartz sensor need to be cut in smaller pieces to fit into the flow cell. After all preparations are completed, the quartzes were rinsed with BO + 1 wt.% FA. At the start of the experiment, the Fe_2O_3 surface is brought into the focus of the microscope. The ongoing processes can be detected as a function of time in the xy-plane (side view) or xz-plane (top view).

RESULTS AND DISCUSSION

Quartz Crystal Microbalance with Dissipation (QCM-D)

Figure 2 shows the resonance frequency shift of the 5th overtone during the deposition of 1 wt.% FA from BO on Fe_2O_3. The shown result is the mean value of 7 measurements between 0 min and 120 min. With the injection of 1 wt.% FA the frequency drops by -1.5 Hz, which indicates a mass increase of 27 ng/cm² (deposition). The results are in good accordance with the results from *Eriksson* [15] and *Nalam et al.* [16]. Interestingly, by changing the medium back to BO the frequency decreases again by -8.8 Hz, which suggests another deposition of 156 ng/cm². Therefore, in total at the end of the test, 183 ng/cm² FA is adsorbed at the Fe_2O_3 surface.

It has been shown that many organic friction modifiers form viscous boundary layers [1]. Therefore, we first calculated a constant layer thickness under the assumption that the density of the adsorbed FA is the same as in the bulk material. The calculated thickness of this layer before rinsing with BO again is 0.27 nm and after rinsing, it amounts to 1.88 nm. As the layer thicknesses are thinner than a monolayer would be, it is likely that FA is not adsorbed as a dense layer but grows as islands. Alternatively, a tilted configuration would be possible.

Figure 3 represents the dissipation shift for the deposition of 1 wt.% FA from BO on Fe_2O_3. Adding 1 wt.% FA leads to a drop in the dissipation shift which equilibrates after a few minutes to a negative dissipation shift of -0.7, which means that the adsorbent is slightly less viscoelastic than the BO. This could be the fact that BO forms a mostly fluid and exchangeable layer at the surface (no or little deposition) while the adsorbed FA is stronger attached to the surface (deposition). The rinsing step with BO increases the dissipation above the initial level by 2.3, which indicates a more viscoelastic behavior and one could initially speculate that the FA has been removed. However, in this case the mass should be decreasing. At this point, it must be pointed out again that the dissipation of the pure base oil is already very high and the changes are comparatively small.

In addition to the mass change and the dissipation shift, the radius can also be determined for nanometer-sized droplet- or bubble-shaped adsorbents [22, 23, 25]. For this purpose, the $\Delta D_n/-\Delta f_n$ - ratio is plotted against the frequency shift $\Delta f/n$. The plot of the negative $\Delta D_n/-\Delta f_n$ - ratio versus the negative frequency shift $\Delta f/n$ for a single measurement of the frequency and dissipation shift for the adsorption of FA from BO is shown in Figure 4. In theory, the slope becomes steeper for larger harmonics [23,26], so that the linear extrapolations of all harmonics converge on an X-axis

intercept. As described in formula 2, the radius r_{QCM} of the adsorbed droplets can be calculated from the negative frequency shift $\Delta f/n$ at $\Delta D_n = 0$ and the Sauerbrey constant c.

For the $\Delta D_n/-\Delta f_n$ ratio shown in Figure 4, the negative linear dependence on the negative frequency shift $\Delta f/n$ is demonstrated with high correlation factors (Pearson R > -0.75). In addition, the slopes of the linear fits become larger for higher harmonics. For n = 3 and n = 5, the slopes are close to each other ($a_{n=3}$ = -0.00105 Hz^{-2} and $a_{n=5}$ = -0.00105 Hz^{-2}), so that the straight lines are approximately parallel. The slopes for n = 7 and n = 9 are also close together ($a_{n=7}$ = -0.00263 Hz^{-2} and $a_{n=9}$ = - 0.00284 Hz^{-2}). The jump between the 5th and 7th overtone causes the linear fits to intersect rather than converge on a common X-axis intercept, so the X-axis intercept scatters over a range from -535 Hz to -183 Hz. On average, it is 307 Hz for the evaluation shown, which corresponds to a radius r_{QCM} of 56 nm with formula 2.

If the calculated radii of all measurements are averaged, a radius r_{QCM} of 41.4 ± 10.5 nm is found for the BO → BO + 1 wt.% FA rinsing step and a radius r_{QCM} of 45.2 ± 3.4 nm for the BO + 1 wt.% FA → BO rinsing step. In the supplementary information, the evaluation of two additional measurements are shown.

Confocal Laser Scanning Microscopy (CLSM)

Rinsing step BO → BO + 1 wt.% FA

Figure 4 depicts the approach and deposition process of a FA droplet emulsified in BO onto the Fe_2O_3 surface in the xz-plane. The grey contrast is due to the reflection signal of the Fe_2O_3 surface at 405 nm. The BO does not fluorescence and FA does show fluorescence at 488 nm and is shown in orange. The representative series of images show a droplet with a diameter of approximately 21 µm approaching the Fe_2O_3 surface. Within 37 seconds, the drop reduces its distance from the

surface before then adsorbing and spreading slightly. The adsorbed droplets appear to be stable afterwards. However, the resolution of the CLSM method does not allow to detect if there is a thinner FA layer between the adsorbed droplets.

Figure 6 is a time series that shows the merging process of two FA droplets in xz-plane. This series was taken during the rinsing with BO + 1 wt.% FA and was observed parallel to the deposition processes shown in Figure 5. A droplet with a diameter of approximately 25 µm is approaching the surface as seen already in Figure 5. This time the droplet does not adsorb at the Fe_2O_3 surface but coalesces with a larger drop (diameter approximately 44 µm), which is already adsorbed at the surface. Since the conditions for deposition and coalescence have been the same and the coalescence has occurred, it can be assumed that this state is preferred in order to reduce the surface energy.

Figure 7 shows the deposition and merging processes of FA droplets in the xy-plane (top view). The greyish background is the Fe_2O_3 surface and the orange droplets are again FA, fluorescent at 488 nm. During the first 4 min a few small droplets (diameters between 0.9 µm and 23 µm) adsorb at the Fe_2O_3 surface (Figure 7a-c). At 05:47 min in the lower right corner, a larger drop appears (Figure 7 d). This droplet is mobile on the surface, but does not desorb. In the next minutes, it moves along the surface (Figure 7e-f). At 13:05 min it merges with an also adsorbed smaller droplet (Figure 7g). We assume that droplets become mobile when they reach a certain volume. They move along the surface and merge with other (mostly smaller) droplets.

Based on geometric considerations, the CLSM-images are used to approximate the measured mass by QCM-D (Figure 7). Since the 5^{th} overtone was used for the analysis of the QCM data, the decay length for the 5^{th} overtone has to be used. For droplets with a radius larger than the decay

length $\delta_{BO + 1\ wt.\%\ FA}$ = 0.58 µm, the cylindrical volume V_{cyl} within the decay length is calculated and multiplied with the density of FA to find the theoretical QCM-D weight per drop $m_{CLSM,\delta}$. Droplets with a radius smaller than the decay length are taken into account with their total half-spherical volume V_{sph} (Figure 7). By adding up the weight of all droplets within the observed area of (400 × 400) µm² to obtain the mass density in ng/cm² can be directly compared to the mass shifts found with QCM-D. The histograms of the radii of the droplets for the time steps 03:00 min and 15:52 min of the image series shown in Figure 6 are given in Figure 8.

The histogram in **Figure 9** shows the radius distribution during rinsing with BO + 1 wt.% FA for the time stamps 3:00 min and 15:52 min in **Figure 7**b+h. After 3:00 min, 11 drops are adsorbed at the surface. The calculated cumulative QCM-D relevant mass increase $\Delta m_{CLSM,\delta}$ here is 244 ng/cm² while the real mass $\Delta m_{CLSM,real}$ is 2553 ng/cm². The ratio of $\Delta m_{CLSM,\delta}$ and $\Delta_{mCLSM,real}$ shows that the QCM could detect a maximum of 0.148% of the real adsorbed mass for the given radius distribution with an average radius of 2.52 µm. After 15:52 min, 13 droplets are adsorbed on the surface. The radius distribution shifts to larger radii, so that the average radius is 4.23 µm. The calculated cumulative mass increase $\Delta_{mCLSM,\delta}$ increases to 413 ng/cm². The value here corresponds to 8% of the real adsorbed mass $\Delta m_{CLSM,real}$. The radius found with QCM-D r_{QCM} is 0,041 µm and therewith, just like the mass, smaller than r_{CLSM}. With the ΔD_n /-Δfn ratio for the QCM-D measurements only 1 % (3:00 min), respectively 0.03 % (15:52 min) of the real radius can be modeled.

From the dissipation shift in the QCM-D measurements (**Figure 3**) it is known that there is a drop directly after changing the medium from BO to BO + 1 wt.% FA. The adsorbing, mostly small droplets decrease the dissipation, so they are less viscoelastic then the initial BO environment. These findings are not intuitive, since one would assume that the droplets increase the

viscoelasticity, as they are liquid and partially mobile. After a few minutes, the dissipation shift stabilizes at a negative value of -0.7. From the histograms in **Figure 9** one can conclude that the number of small droplets is shrinking at the expense of the large ones, which would indicate, that bigger drops are more viscoelastic than smaller ones.

Rinsing step BO + 1 wt.% FA → BO

Figure 10 depicts a series of images when rinsing the Fe_2O_3 surface with BO again, after rinsing with BO + 1 wt.% FA, in xy-plane. In the initial state, so during rinsing with BO + 1 wt.% FA, 5 bigger droplets (diameters between 88 µm and 127 µm) and a few smaller ones (diameters < 1 µm) are adsorbed on the surface, which correspond to a surface coverage of 5.9 %. Due to rinsing with BO the amount of adsorbed FA droplets increase. In addition to the droplets already present in the initial state, there are now a higher number of smaller droplets (diameters < 1 µm) on the surface and the surface coverage increases to 6.6 %.

Using the same approach to calculate the theoretical masses from the CLSM as described above (compare **Figure 8**) for the initial state at time 1:32 min we obtain a QCM-D relevant mass of $\Delta m_{CLSM,\delta}$ of 3310 ng/cm² and a real adsorbed mass $\Delta m_{CLSM,real}$ of 1,6E6 ng/cm². The corresponding histogram is shown in **Figure 11**. For the given radius distribution, 3.6% of the real adsorbed mass of the droplets are detected by the QCM-D. The masses calculated from the CLSM images here are significantly higher than the masses from calculated for the rinsing step BO → BO + 1 wt.% FA.

Since the FA droplets are distributed inhomogeneously on the Fe_2O_3 surface, a larger number of measurements in different measurements areas is necessary to generate a representative average value. Within the scope of this work, only the measurement ranges shown could be investigated.

The average value, which is not very expressive, is 1862 ± 1449ng/cm². In comparison, the mass Δm_{QCM} determined with the QCM-D is only 27 ng/cm². It is known from the literature that the simplified calculation with the Sauerbrey equation leads to underdetermined masses due to the high dissipation level (not dissipation shift). The ratio $\frac{\Delta m_{QCM}}{\Delta m_{CLSM,\delta}}$ can be considered as a correction to the Sauerbrey constant c, so that an effective constant $c_{eff} = \frac{c}{c_{cor}}$ can be given for the adsorbed FA droplets. Since the deviation of the masses depends on the distribution function of the radii X(r) of the droplets, the corrected Sauerbrey "constant" c_{cor} must be given as a function of the distribution function of the radii X(r), so that a dependence of the distribution function of the radii X(r) also results for the effective "constant" ($c_{eff}(r) = \frac{c}{c_{cor}(X(r))}$). Based on the limited data available, no model will be developed at this point.

After rinsing with BO for another 2 min, (cf. Figure 4d at 3:10 min), the droplet number increases to 23. The calculated cumulative mass increase $\Delta m_{CLSM,\delta}$ is 3694 ng/cm². The measured mass from the QCM-D measurement Δm_{QCM} for the same condition is about 95% lower, i.e. 183 ng/cm².

The dissipation shift for the change from BO + 1 wt.% FA to BO was found to be 2.3 (Figure 3). The additional deposition of droplets thus not only results in an increase in mass, but also increase the viscoelasticity. The histograms in Figure 11 show that mostly small droplets with a radius < 5 µm additionally adsorb. The results found for the rinsing step with BO + 1 wt.% FA (described above) showed, that smaller drops are less viscoelastic than bigger ones. Here it turns out that a larger amount of smaller drops are more viscoelastic than less bigger drops (compare the histogram in Figure 11). It is evident that the distribution and the size of the droplets and their interrelations are necessary to describe the dissipations shifts found with QCM-D.

A possible explanation for the additional deposition during rinsing with BO and therewith rinsing the Fe_2O_3 surface with a less concentrated emulsion, we consider the solubility of FA in BO. During the rinsing process, adsorbed droplets could be released from the tubes and walls of the cell and adsorb on the Fe_2O_3 surface instead. As a result, more mass is detected by the QCM-D.

CONCLUSIONS

Using QCM-D the frequency shift was measured and the corresponding mass was calculated using the Sauerbrey equation. It was found that the adsorbent, which basically is FA, adsorbs with 27 ng/cm². As the resulting layer thickness of 0.27 nm is less than a monolayer, island growth can be assumed. Indeed CLSM measurements surprisingly show that the additive forms droplets in the base oil, which stick onto the Fe_2O_3 surface, which contradicts the common assumption that friction modifiers form dense films. By recording CLSM videos, it was for the first time possible to observe the deposition of FA droplets from BO on Fe_2O_3 surfaces in-situ. The adsorbed FA droplets have radii varying between 0.4 µm and 14.5 µm. With QCM-D the radii were determined using the $\Delta D_n/-\Delta f_n$ - ratio. With a mean value of 43 nm the calculated radii are one order of magnitude smaller than the real radii found with CLSM. By adding up the weight of all droplets within the measurement area (400 x 400) µm² and recalculated the value to ng/cm² the values were compared with the mass shifts found with QCM-D. The mean value of both areas rinsed with BO + 1 wt.% is 1860± 1448 ng/cm². The high uncertainty is due to the low number of random sampling and the fact that the FA droplets are non-homogeneously distributed on the Fe_2O_3 surface and thus the results strongly depend on the investigated area. Just as for mass determination, the radii determined with the QCM-D are significantly smaller than those measured with CLSM.

The correlation of the CLSM results and the dissipation shift found with QCM-D is not intuitive. The deposition of FA droplets lowers the viscoelasticity, even though the droplets are liquid and partially mobile. Finally, it is important to realize that the number, the distribution and the size of the droplets and their interrelations are relevant parameters to describe the dissipation shifts found with QCM-D alone. For this reason, the combination of CLSM and QCM-D can be very valuable.

Another interesting observation of the FA was found during the rinsing step with BO + 1 wt.% FA. Parallel to deposition processes, merging of droplets was observed. If the conditions for deposition and coalescence are the same, coalescence occurs. This indicates that FA prefers the state of an emulsion not only over the solution in BO but also over deposition on Fe_2O_3 surface. If droplets deposit on the surface they are not mobile until they reach a certain volume. Larger droplets are mobile, move along the surface, and merge with other (mostly smaller) droplets.

Rinsing the Fe_2O_3 surface with already adsorbed FA droplets with BO again, diluting the emulsion, interestingly leads to a second deposition step. With QCM-D, the additionally adsorbed mass was found to be 156 ng/cm². As a result at the end of the test, 183 ng/cm² FA is adsorbed at the Fe_2O_3 surface. With CLSM we could not reproduce this phenomenon quantitatively, as the additionally amount adsorbed in the investigated area was significantly higher at 1E05 ng/cm². Qualitatively, the additional deposition was confirmed by CLSM as the number of mainly smaller droplets increases during rinsing with BO.

FIGURES

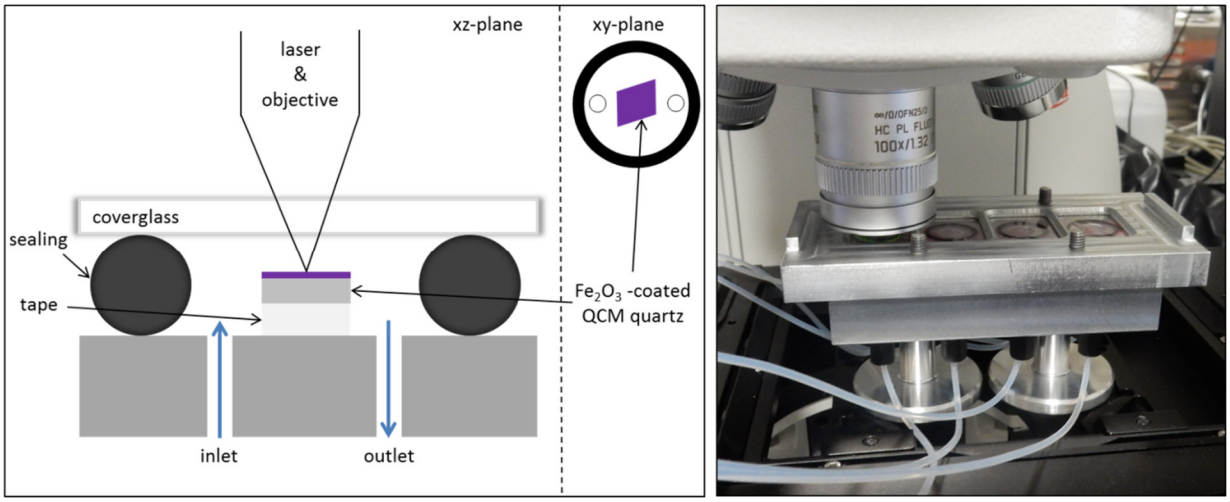

Figure 1. Schematic and photo of the measurement setup with flow cell under the CLSM.

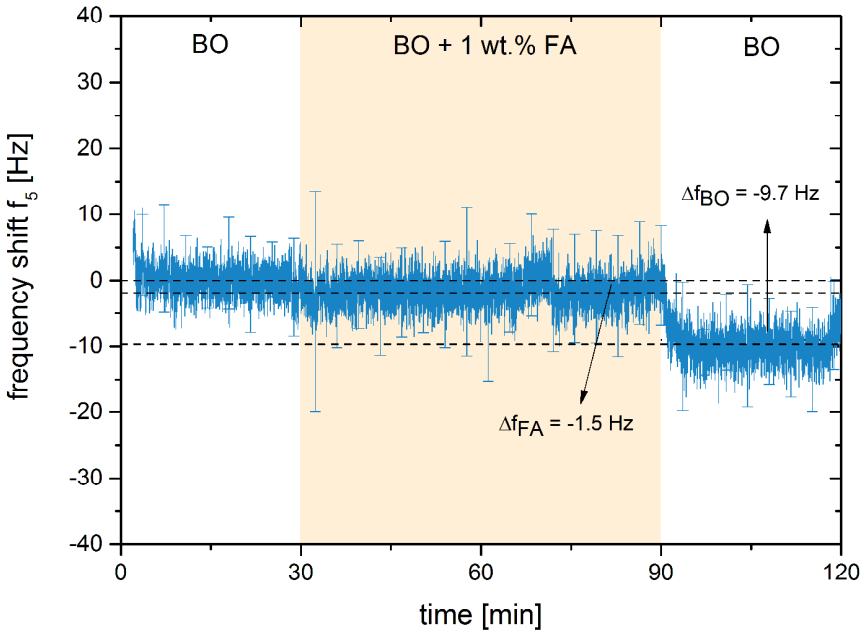

Figure 2. Mean value of QCM-D measurements of FA deposition from BO (frequency signal of 5th overtone); results shown for BO rinsing 0 – 30 min, BO + 1 wt.% FA rinsing 30 – 90 min and BO rinsing 90 – 120 min; error bars are standard deviation of 7 single measurements.

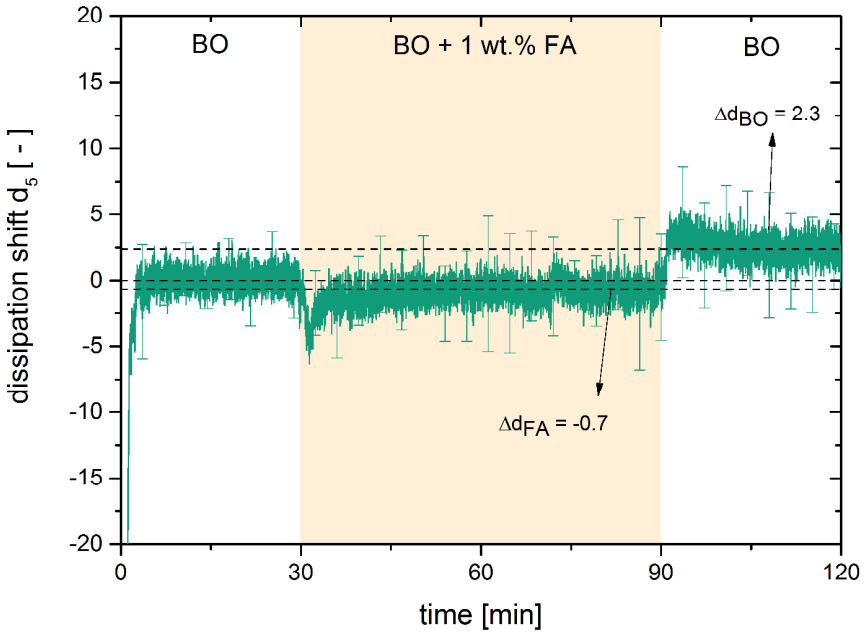

Figure 3. Mean value of QCM-D measurements of FA deposition from BO (dissipation signal of 5th overtone); results shown for BO rinsing 0 – 30 min, BO + 1 wt.% FA rinsing 30 – 90 min and BO rinsing 90 – 120 min; error bars are standard deviation of 7 single measurements

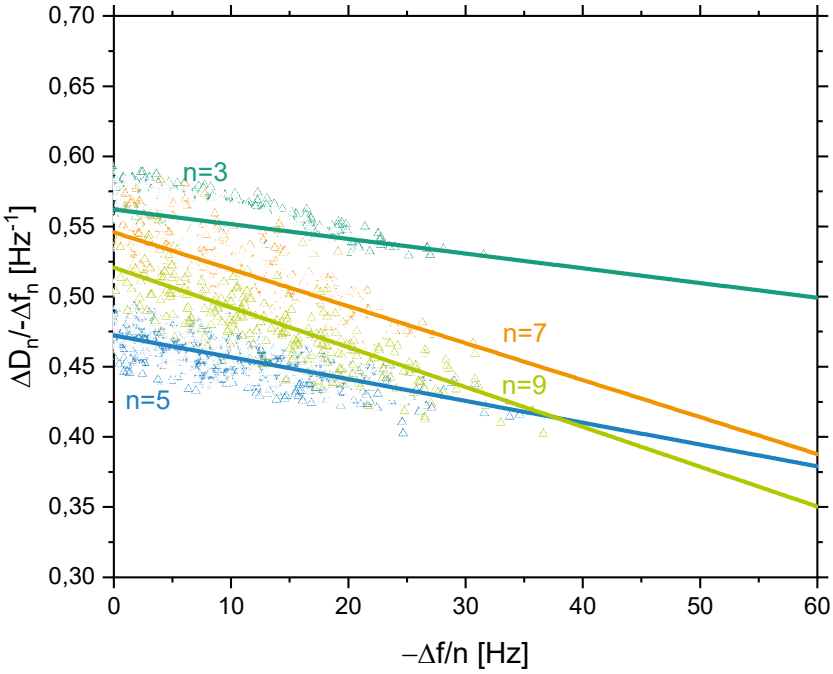

Figure 4 $\Delta D_n/-\Delta f_n$ - ratio plotted against the frequency shift Δf/n for a single measurement during the rinsing step BO → BO + 1 wt.% FA (20 - 50 min)

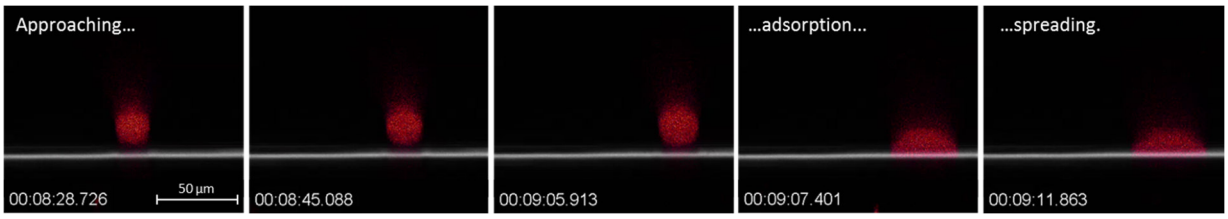

Figure 5. CLSM recording of the deposition of a droplet of friction modifier in xz-plane. The reflection signal at 405 nm in grey represents the Fe_2O_3 surface, above the crystal a mixture of BO + 1 wt.% FA flows through the surface with a flow rate of approximately 140 µl/min. BO does not fluoresces (no signal), FA fluoresces at 488 nm (orange), the format of the timestamp is hh:mm:ss:mss.

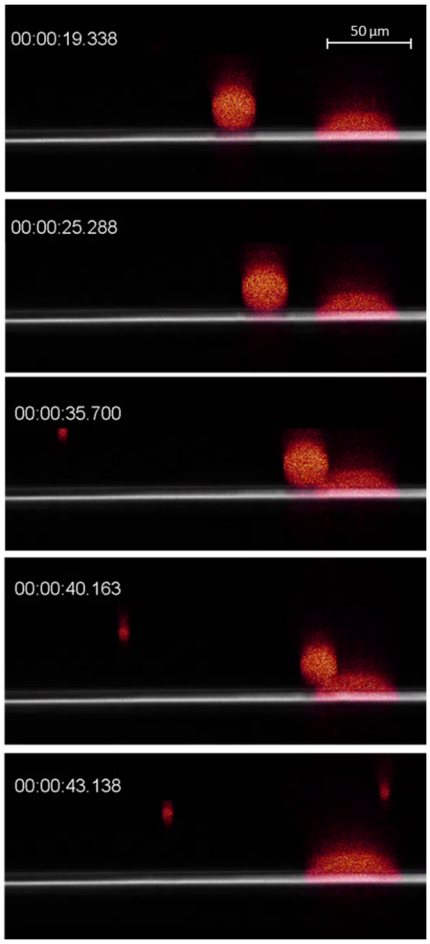

Figure 6. CLSM recording of two merging droplets of friction modifier in xz-plane. The reflection signal at 405 nm in grey represents the Fe_2O_3 surface, above the crystal a mixture of BO + 1 wt.% FA flows through the surface with a flow rate of approximately 140 µl/min. BO does not fluoresces (no signal), FA fluoresces at 488 nm (orange). The format of the timestamp is hh:mm:ss:mss.

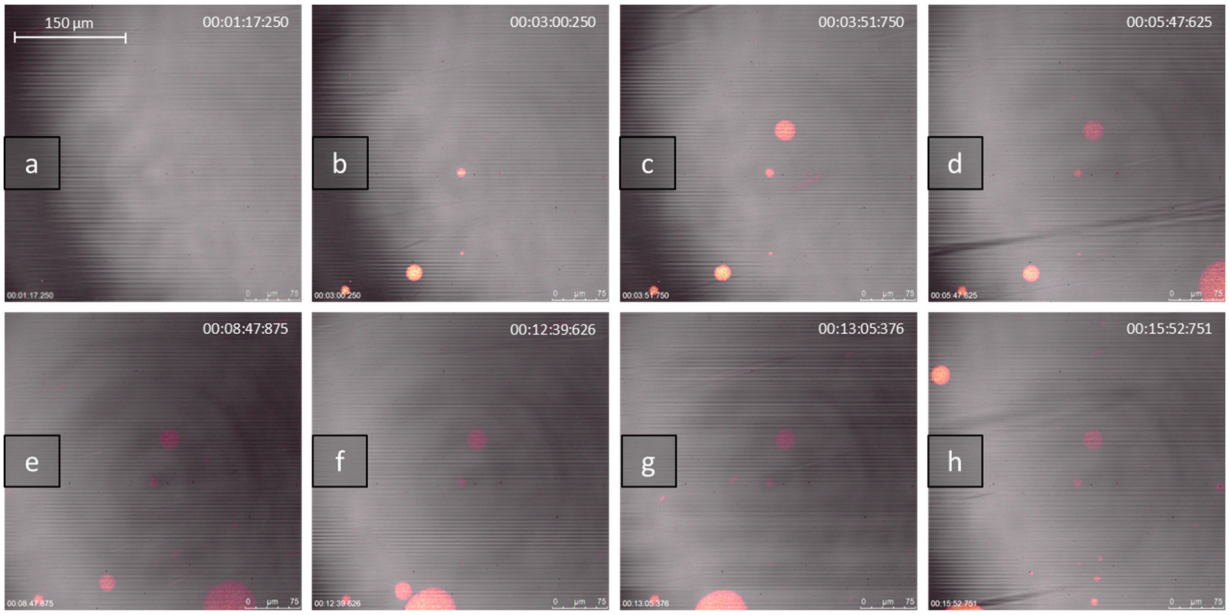

Figure 7. CLSM recording of the deposition of droplets of friction modifier in xy-plane. The reflection signal at 405 nm in grey represents the Fe_2O_3 surface, above the crystal a mixture of BO + 1 wt.% FA flows through the surface with a flow rate of approximately 140 µl/min. BO does not fluoresces (no signal), FA fluoresces at 488 nm (orange). The format of the timestamp is hh:mm:ss:mss.

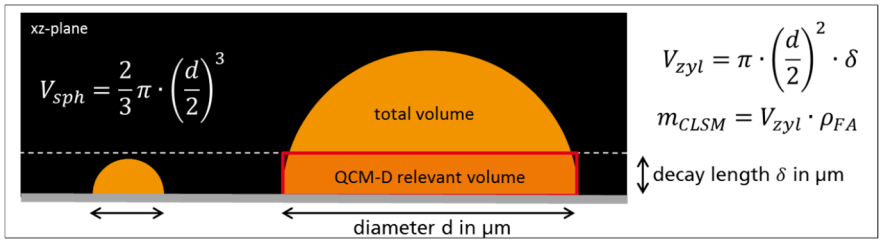

Figure 8. Schematic drawing of adsorbed droplet in xz-plane and used equations.

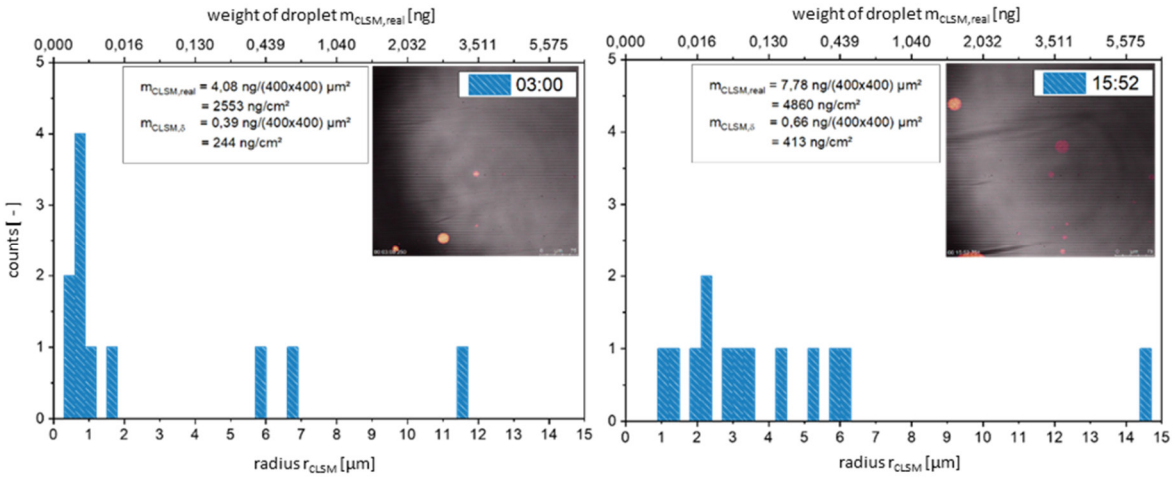

Figure 9. Distribution of radii for time steps 3:00 and 15:52 (compare Figure 7) during rinsing with BO + 1 wt.% FA (size of class 0.3 µm). The given masses are calculated by adding up the weight of all droplets within the area 400 x 400 µm². Format of the timestamp is mm:ss.

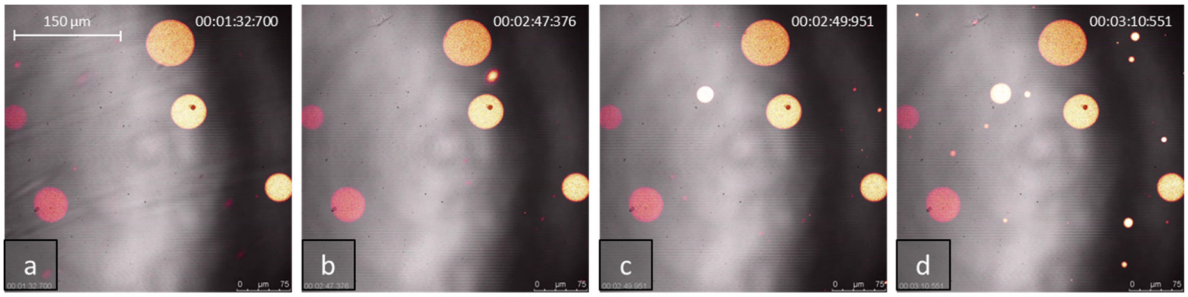

Figure 10. CLSM recording of the deposition of a droplet of friction modifier in xy-plane initially during rinsing with BO. The reflection signal at 405 nm in grey represents the Fe2O3 surface, above the crystal a mixture of BO + 1 wt.% FA flows through the surface with a flow rate of approximately 140 µl/min. BO does not fluoresces (no signal), FA fluoresces at 488 nm (orange). The format of the timestamp is hh:mm:ss:mss.

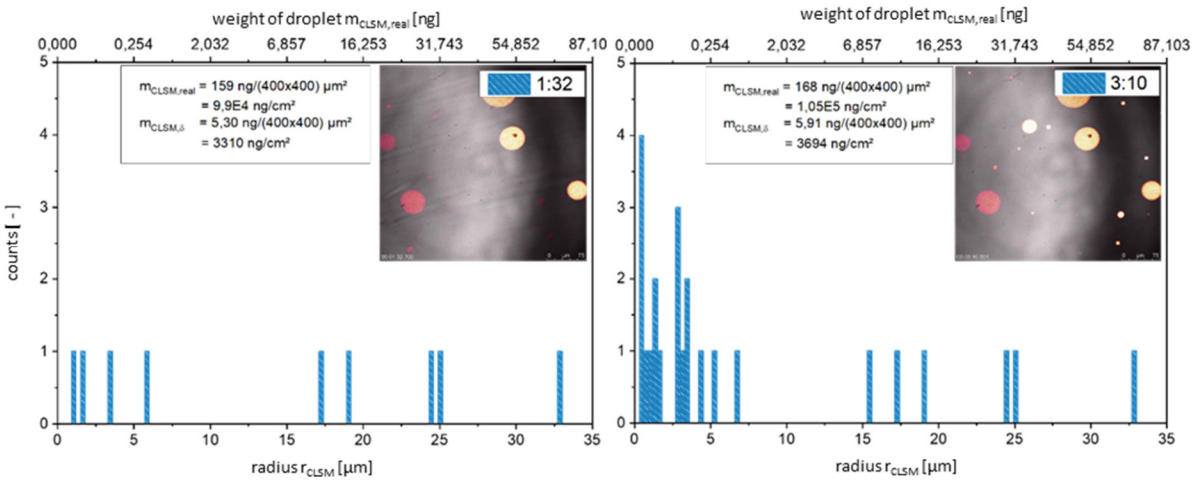

Figure 11. Distribution of radii for time steps 1:32 and 3:10 (compare Figure 10) during rinsing with BO (size of class 0.3 µm). The given masses are calculated by adding up the weight of all droplets within the area 400 x 400 µm².The format of the timestamp is mm:ss.

TABLES

Table 2. Physical properties of FA, BO and BO + 1 wt.% FA

	FA	BO	BO + 1 wt.% FA
kinematic viscosity [mm²/s]	290 (20 °C)	25.48 (55 °C)	25.94 (55°C)
density [g/cm³]	0.97 (20 °C)	0.84 (55 °C)	0.84 (55°C)

FA denotes the friction modifier additive, the properties of the base oil are denoted with BO

AUTHOR INFORMATION

Corresponding Author

*Corresponding Author: martin.dienwiebel@kit.edu

Author Contributions

The manuscript was written through contributions of all authors. All authors have given approval to the final version of the manuscript.

ACKNOWLEDGMENT

The authors acknowledge the assistance by D. Bahl and S. Janson with the CLSM measurements and M. Rückel for the discussion of the results. M.D. acknowledges the Deutsche Forschungsgemeinschaft (DFG) under grant DI1494/4-1.

REFERENCES

(1) Spikes, H. Friction Modifier Additives. Tribol Lett 2015, 60, 119–145.

(2) Tang, Z.; Li, S. A review of recent developments of friction modifiers for liquid lubricants (2007–present). Current Opinion in Solid State and Materials Science 2014, 18, 119–139.

(3) Bowden, F. P.; Gregory, J. N.; Tabor, D. Lubrication of Metal Surfaces by Fatty Acids. Nature 1945, 156, 97–101.

(4) Daniel, S. G. The adsorption on metal surfaces of long chain polar compounds from hydrocarbon solutions. Trans. Faraday Soc. 1951, 47, 1345–1359.

(5) Loehle, S.; Matta, C.; Minfray, C.; Le Mogne, T.; Martin, J.-M.; Iovine, R.; Obara, Y.; Miura, R.; Miyamoto, A. Mixed Lubrication with C18 Fatty Acids: Effect of Unsaturation. Tribology Letters 2014, 53, 319–328.

(6) Campen, S.; Green, J. H.; Lamb, G. D.; Spikes, H. A. In Situ Study of Model Organic Friction Modifiers Using Liquid Cell AFM; Saturated and Mono-unsaturated Carboxylic Acids. Tribol Lett 2015, 57, 51-71.

(7) Kuwahara, T.; Romero, P. A.; Makowski, S.; Weihnacht, V.; Moras, G.; Moseler, M. Mechano-chemical decomposition of organic friction modifiers with multiple reactive centres induces superlubricity of ta-C. Nature Communications 2019, 10, 151.

(8) Bernat, S.; Armada, S.; Espallargas, N. Friction Mechanisms by Carboxylic Acids in Aqueous Lubricants. Tribology Letters 2018, 66, 82-97.

(9) Hardy, W. B.; Doubleday, I. Boundary lubrication.— The paraffin series. Proceedings of the Royal Society of London. Series A, Containing Papers of a Mathematical and Physical Character 1922, 100, 550–574.

(10) Benítez, J. J.; Kopta, S.; Ogletree, D. F.; Salmeron, M. Preparation and Characterization of Self-Assembled Monolayers of Octadecylamine on Mica Using Hydrophobic Solvents. Langmuir 2002, 18, 6096–6100.

(11) Zhu, Y.; Ohtani, H.; Greenfield, M. L.; Ruths, M.; Granick, S. Modification of Boundary Lubrication by Oil-Soluble Friction Modifier Additives. Tribology Letters 2003, 15, 127–134.

(12) Wood, M. H.; Welbourn, R. J. L.; Charlton, T.; Zarbakhsh, A.; Casford, M. T.; Clarke, S. M. Hexadecylamine adsorption at the iron oxide-oil interface. Langmuir 2013, 29, 13735–13742.

(13) Doig, M.; Camp, P. J. The structures of hexadecylamine films adsorbed on iron-oxide surfaces in dodecane and hexadecane. Phys. Chem. Chem. Phys. 2015, 17, 5248–5255.

(14) Gidalevitz, D.; Huang, Z.; Rice, S. A. Urease and hexadecylamine-urease films at the air-water interface: an x-ray reflection and grazing incidence x-ray diffraction study. Biophys J 1999, 76, 2797–2802.

(15) Eriksson, K. Fatty Amines as Friction Modifiers in Engine Oils: Correlating Adsorbed Amount to Friction and Wear Performance. Master Thesis, Chalmer University of Technology, Gothenburg, Schweden, 2014.

(16) Nalam, P. C.; Pham, A.; Castillo, R. V.; Espinosa-Marzal, R. M. Adsorption Behavior and Nanotribology of Amine-Based Friction Modifiers on Steel Surfaces. The Journal of Physical Chemistry C 2019, 123, 13672–13680.

(17) Jung, A. K.; Voelkel, L; Crema, S. European Patent No. EP 2321389B1

(18) Sauerbrey, G. Verwendung von Schwingquarzen zur Wägung dünner Schichten und zur Mikrowägung. Zeitschrift für Physik 1959, 155, 206–222.

(19) Qiao, X.; Zhang, X.; Tian, Y.; Meng, Y. Progresses on the theory and application of quartz crystal microbalance. Applied Physics Reviews 2016, 3, 31106.

(20) Rodahl, M.; Kasemo, B. Frequency and dissipation-factor responses to localized liquid deposits on a QCM electrode. Sensors and Actuators B: Chemical 1996, 37, 111–116.

(21) Evans, K. O. Quartz crystal microbalance investigation of the structure of adsorbed soybean oil and methyl oleate onto steel surface. Thin solid films 2010, 519, 900-905.

(22) Reviakine, I.; Johannsmann, D.; Richter, R. P. (2011): Hearing what you cannot see and visualizing what you hear: interpreting quartz crystal microbalance data from solvated interfaces. In: Analytical chemistry 83 (23), S. 8838–8848. DOI: 10.1021/ac201778h.

(23) Johannsmann, D. (2015): The Quartz Crystal Microbalance in Soft Matter Research. Fundamentals and Modeling. Cham: Springer (Soft and Biological Matter). DOI: 10.1007/978-3-319-07836-6.

(24) Reviakine, I.; Gallego, M.; Johannsmann, D.; Tellechea, E. (2012): Adsorbed liposome deformation studied with quartz crystal microbalance. In: The Journal of chemical physics 136 (8), S. 84702. DOI: 10.1063/1.3687351.

(25) Tellechea, E.; Johannsmann, D.; Steinmetz, N. F.; Richter, R. P.; Reviakine, I. (2009): Model-independent analysis of QCM data on colloidal particle adsorption. In: Langmuir : the ACS journal of surfaces and colloids 25 (9), S. 5177–5184. DOI: 10.1021/la803912p.

(26) Grunewald, C.; Schmudde, M.; Noufele, C. N.; Graf, C.; Risse, T. (2015): Ordered Structures of Functionalized Silica Nanoparticles on Gold Surfaces: Correlation of Quartz Crystal Microbalance with Structural Characterization. In: Analytical chemistry 87 (20), S. 10642–10649. DOI: 10.1021/acs.analchem.5b03572.

Graphical Abstract

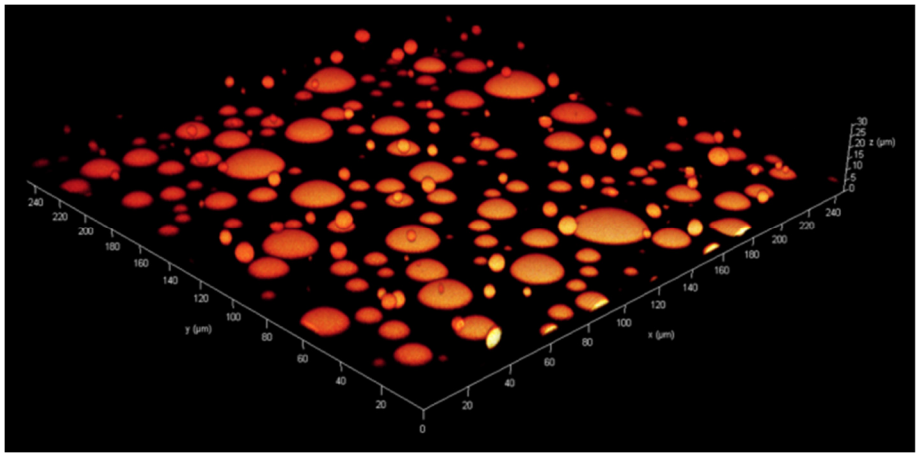

Supplementary Information

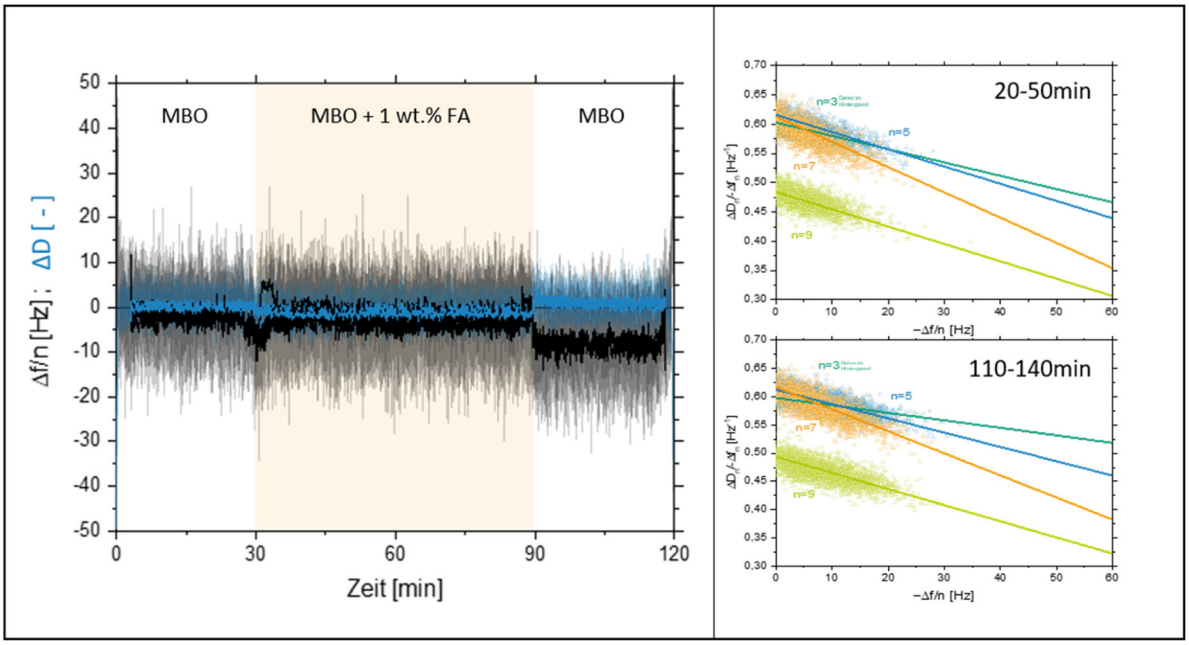
MBO
MBO + 1 wt.% FA
MBO
Δf/n [Hz] ; ΔD [-]
Zeit [min]
20-50min
110-140min
n=3
n=5
n=7
n=9
−Δf/n [Hz]

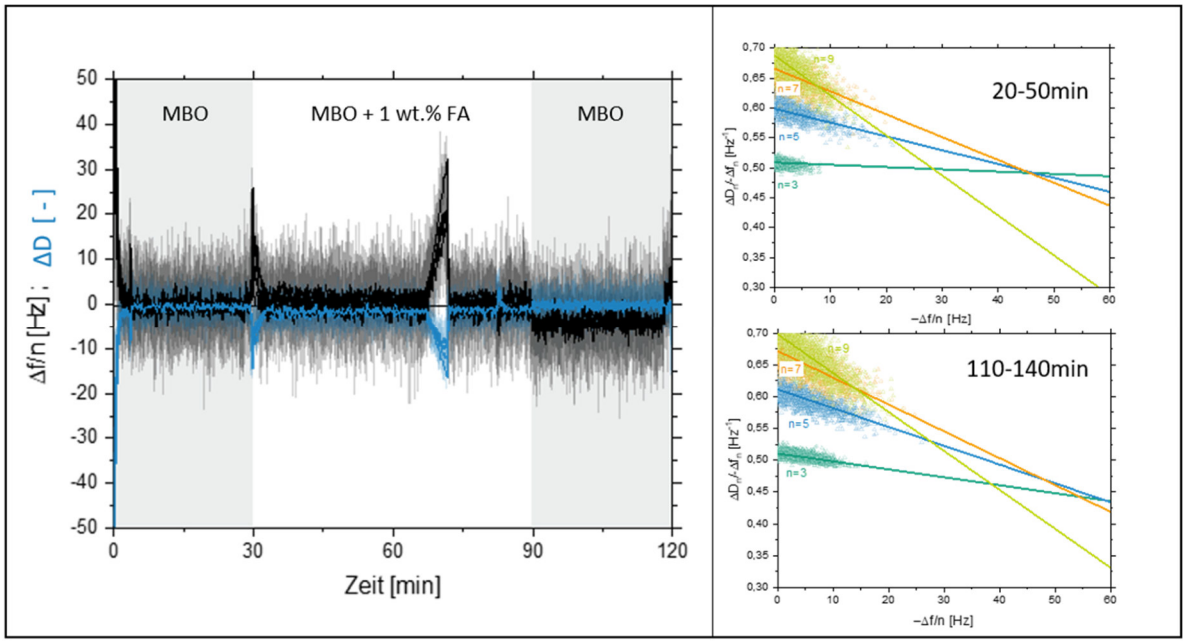
MBO
MBO + 1 wt.% FA
MBO
Δf/n [Hz] ; ΔD [-]
Zeit [min]
20-50min
110-140min
n=3
n=5
n=7
n=9
−Δf/n [Hz]